ORIGINAL PAPER: SOL-GEL AND HYBRID MATERIALS FOR CATALYTIC, PHOTOELECTROCHEMICAL AND SENSOR APPLICATIONS

Synthesis of N-F-codoped TiO$_2$/SiO$_2$ nanocomposites as a visible and sunlight response photocatalyst for simultaneous degradation of organic water pollutants and reduction of Cr (VI)

Sina Ghanbari[1] · Mohammad Hadi Givianrad[1] · Parviz Aberoomand Azar[1]

Abstract

A new N-F-codoped TiO$_2$/SiO$_2$ nanocomposite was prepared by simple sol-gel method, and strongly stabilized on a substrate used in a fabricated photoreactor. The prepared photocatalysts were characterized by X-ray diffraction, Fourier-transform infrared spectroscopy, diffuse reflectance UV/Vis, photoluminescence, field emission scanning electron microscope, energy dispersive X-ray, transmission electron microscope, and N$_2$ adsorption/desorption methods. The effective parameters of pH, flow rate of the incoming current, and the photoreactor tubes angle against sunlight were optimized. The photocatalytic performance of prepared photocatalysts was evaluated by studying the simultaneous removal of a mixture containing three azo dyes and Cr (VI) in the fabricated continuous-flow photoreactor under visible and solar irradiation. The performance of the designed system was also proved under various outdoor climate conditions. Total organic carbon and flame atomic absorption spectroscopy analysis were performed on the treated sample to confirm the decontamination of the model pollutant mixture. It was found that doping N and F in TiO$_2$/SiO$_2$ nanoparticles caused least agglomeration, enhanced activity under visible and solar irradiation, and fully anatase crystalline structure in the as-synthesized nanoparticles.

Graphical Abstract
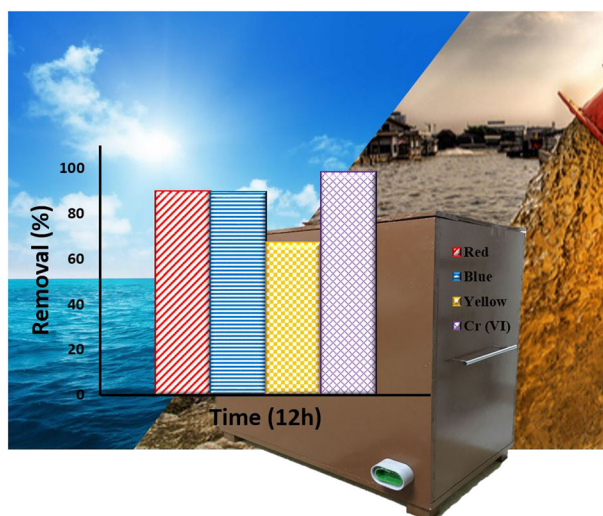
✉ Mohammad Hadi Givianrad
   givianradh@yahoo.com

1 Department of Chemistry, Science and Research Branch, Islamic
   Azad University, Tehran, Iran

Highlights

- N-F-codoped TiO$_2$/SiO$_2$ nanocomposites were synthesized using a simple sol-gel process.
- The nanocomposites were stabilized on the glass beads' surface by coupling two coating methods.
- A photoreactor with adjustable effective parameters was fabricated.
- The photoremovals were successfully tested on a mixture of some organic and inorganic pollutants.
- Different outdoor climate conditions were efficaciously investigated.

1 Introduction

Nanosized TiO$_2$ is one of the most promising photocatalysts for degradation of organic water pollutants [1–5]. Between three polymorphs of TiO$_2$ (rutile, brookite, and anatase), the most activated one in the photocatalytic process is anatase [6, 7]. However, its wide band gap (3.2 eV) makes it inactive under visible light irradiation [2, 3, 8]. One of the most promising methods for improving TiO$_2$ activity under visible and solar light irradiation is doping with non-metals like N, C, B, and F [9, 10]. Among them, nitrogen seems to be the most efficient and the most investigated dopant between others. Asahi et al.'s [11, 12] revolutionary work showed that sputtering TiO$_2$ targets in an N$_2$/Ar gas atmosphere showed a red shift in absorption spectrum of TiO$_2$ and decolorized methylene blue. Doping two different elements such as B and N [13, 14], Ni and Pt [15, 16], S and N [17–19], N and F [2, 20] have resulted to enhanced effect on the photocatalytic activity of the prepared nanoparticles under visible and solar irradiation. Wu et al. [2] prepared a nitrogen and fluorine codoped mesoporous TiO$_2$ microspheres to photocatalytic degradation of Acid Orange 7 under visible light. Xie et al. [20] synthesized F-N-codoped TiO$_2$ at low temperature condition activated under visible light using TiCl$_4$ and NH$_4$F and examined molar ratios of N and F dopants. Wang et al. used N and F codoped TiO$_2$ to reduce hexavalent chromium under visible light and showed that doping both nitrogen and fluorine on TiO$_2$ is more beneficial than N-doped or F-doped TiO$_2$, because N-doping causes red shift in absorption wavelength and F-doping results less agglomeration of nanoparticles [2]. Pang et al. [21] synthesized N-F-codoped TiO$_2$/SiO$_2$ for decomposition of acrylonitrile under solar light with mesoporous structure. Mixing SiO$_2$ into TiO$_2$ lattice investigated by Anderson et al. and showed enhanced activity in destruction of rhodamine-6G than TiO$_2$ alone [22]. Mahesh et al. [23] used PU-TiO$_2$/SiO$_2$ hybrid composite films for degradation of Acid Black 1 and reported that incorporating TiO$_2$ and SiO$_2$ increased the thermal stability and degradation temperature of the prepared nanocomposite. Islam et al. [24] prepared a crack-free sol-gel based TiO$_2$/SiO$_2$ hybrid nanoparticle films that resulted to homogeneous and less-aggregated surface.

Herein, in this study, the sol-gel method was used and dip-coating process followed by heat attachment method to immobilize N-F-codoped TiO$_2$/SiO$_2$ (NFTS) on glass beads and examined decolorization of three azo dyes and reduction of Cr (VI) in a fabricated photoreactor under visible and solar irradiation. It was found that codoped TiO$_2$/SiO$_2$ by nitrogen and fluorine yielded to much higher photocatalytic activity than pure TiO$_2$.

2 Experimental

2.1 N-F-sol preparation

All the chemicals were purchased from Merck and used as received without any further purification. The TiO$_2$/SiO$_2$ sol was synthesized in acidic condition by hydrolyzing titanium (IV) n-butoxide (TNBT). In this method, 5 mL TNBT, 20 mL ethanol, and 5 mL acetylacetone were mixed together under vigorous stirring for 30 min. Then 4.0 mL double distilled water was added dropwise and stirring continued for another 10 min. Afterwards, the pH of the solution was adjusted about 1.7 with concentrated HCl. In the next step, the appropriate amount of urea (CH$_4$N$_2$O) as nitrogen source and ammonium fluoride (NH$_4$F) as fluorine source was added to the solution while stirring. After vigorous stirring for 2 h, 2 g extra pure silica gel 60 (70–230 mesh) was added to the solution and the solution stirred for the next 2 h. The molar ratio of the dopants to the titanium source was 2:1 for urea and 0.1:1 for ammonium fluoride and was investigated in previous researches [20, 21, 25].

2.2 Photocatalyst immobilization on glass beads

Prior to coating process, the glass beads (~ 1 mm in diameter) were cleaned with detergent and etched in diluted hydrofluoric acid for 24 h to prepare the suitable surface porosity for deposition of thin films. In the next step after washing with deionized water, the beads were placed in an oven at 100 °C for 2 h. In this study, dip-coating method followed by heat attachment method were used to immobilize nanoparticles on the glass beads to gain more stability of the particles. According to dip-coating method, the beads

were immersed in the sol for the first 30 min. After drying them with the blow dryer, dipping repeated for the next 30 min. After drying and immersing for another 30 min, the coated glass beads were placed in oven at 100°C for 4 h. At the next step, the immobilized glass beads were calcinated in furnace at 500°C for 1 h to yield NFTS nanocomposites. To improve the stability of the as-prepared substrates, heat attachment method was used followed by heating at 150°C for 2 h. Subsequently, undoped TiO$_2$ nanocomposites were obtained as mentioned procedure.

2.3 Evaluation of photocatalytic activity of the as-synthesized samples

The photocatalytic activity of NFTS was measured using three azo dyes including Basic red 29, Basic blue 41, Basic yellow 51, and K$_2$Cr$_2$O$_7$ as a Cr (VI) source. The photocatalytic degradation was carried out in a fabricated photoreactor under visible and solar light. This photoreactor was consisted of seven glass tubes ($L = 20$ cm, ID $= 1$ cm) on a reflective surface equipped with a peristaltic pump and a black box to prevent UV leakage. The visible source was an OsramPowerstar® HQI®-BT 400 W/D Pro metal halide lamp with a UV cutoff filter and the distance of the visible source were fixed at 10 cm in all experiments. The spectral power distribution of the applied visible source was shown in Fig. 1. The direction of the photoreactor tubes in front of sun irradiation was also adjustable in 30°, 45°, and 60° angles against the vertical line. A volume of 1000 mL mixture containing 30 mg L^{-1} of model colors and 5 mg L^{-1} hexavalent chromium source was mixed and adequate volume of the mixture was taken periodically to investigate the removal process. The detection process was performed via UV/Vis spectrophotometer based on their corresponding λ_{max}. To eliminate the interference of dyes, determining of Cr (VI) reduction was performed by 1,5-diphenylcarbazide method followed by subtracting method at 544 nm [3, 26, 27]. Hence, Cr (VI) measurement was accomplished using two different solutions containing 1,5-diphenylcarbazide/

acetone/water denoted as ternary solution and acetone/water mixture denoted as binary solution. To do this, 2 mL sample, 500 μL H$_2$SO$_4$, and 1 mL of ternary solution were mixed and the immediately formed complex was measured spectrophotometrically at 544 nm (A_1). Then, another 2 mL of the sample at the same related time was mixed with 500 μL H$_2$SO$_4$ and 1 mL binary solution. The absorbance of the sample was measured at 544 nm (A_2). Subsequently, total absorbance of the purple complex of Cr (VI) (A_t) was measured as follows:

$$A_t = A_1 - A_2 \tag{1}$$

2.4 Catalyst characterization

The X-ray diffraction (XRD) pattern of the prepared catalysts was determined by an X-ray diffractometer (Seifert 3003 PTS) using Cu Kα as X-ray source in the 2θ range of 15−90°. The average crystallite size of anatase phase was determined according to Scherrer equation. The Fourier-transform infrared spectroscopy (FT-IR) spectra of the samples were obtained on a Thermo Nicolet 870 Spectrometer. The photoluminescence (PL) spectra of the samples was determined on a Cary Eclipse spectrometer. The diffuse reflectance UV/Vis (DRS-UV/Vis) spectra of the samples were measured on Avantes Avaspec-2048-TEC spectrometer. The morphology and size of nanoparticles were characterized using a field emission scanning electron microscope (FESEM) equipped with an energy dispersive X-ray (MIRA3 TESCAN-XMU). Transmission electron microscope (TEM) Philips (CM30 at 150 KV) was used to observe the images of prepared nanoparticles. The nitrogen adsorption/desorption isotherms were determined via Belsorp mini II; and the specific surface area and pore size distribution from the adsorption branch were measured using Brunauer-Emmett-Teller (BET) and Barret-Joyner-Halender (BJH) methods, respectively. The degradation process of the pollutants was controlled by a Varian Cary300 UV/Vis spectrophotometer. Afterward, total organic carbon of the treated and untreated samples was measured by Hach DR5000 spectrophotometer and total chromium of the treated samples was determined by Varian SpectraAA200 spectrometer.
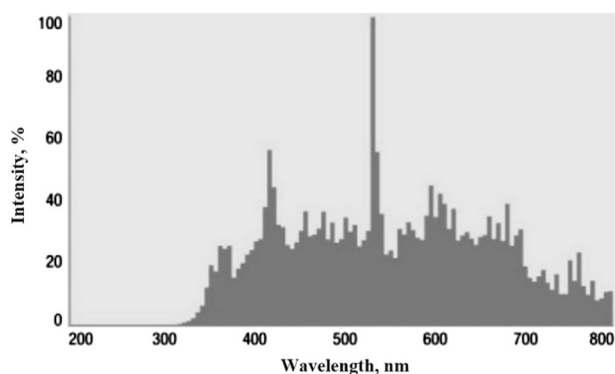
3 Results and discussion

3.1 XRD analysis

The XRD patterns of the prepared samples were shown in Fig. 2. Anatase is the most activated TiO$_2$ polymorph in photocatalytic process [6, 28]. The anatase phase of TiO$_2$ in
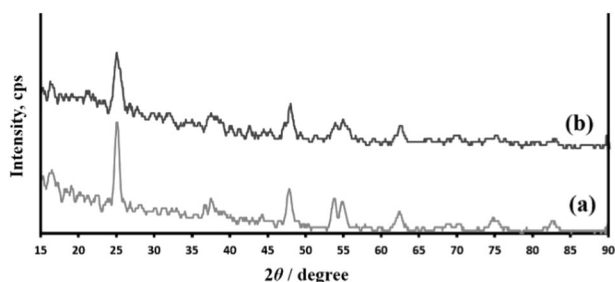

Fig. 1 Spectral power distribution of the applied visible light source

Fig. 2 XRD pattern of undoped TiO_2 **a** and NFTS **b**

the XRD patterns has a main peak in $2\theta = 25.2°$ according to the JCPDS No. $21-1272$ and the results showed the fully anatase structure of the prepared nanocomposites [29]. The grain size of the as-synthesized nanoparticles was estimated by Scherrer equation at the anatase main peak:

$$D = \frac{0.89\lambda 180}{\pi\beta Cos\theta} \tag{2}$$

where D is the crystal size of the nanoparticle, λ is the X-ray wavelength, β is the full width at half maximum of the diffraction peak in radian. Average crystal sizes of pure TiO_2 and NFTS were calculated as 11.33 nm and 6.40 nm, respectively. As it is obvious, doping nitrogen and fluorine was significantly reduced the crystalline growth which was yielded to smaller particle size and higher catalytic activity due to its greater interaction with the pollutant molecules.

3.2 FT-IR spectroscopy analysis

The FT-IR spectra of the prepared samples was shown in Fig. 3. The peaks related to stretching vibrations of O-H and bending vibration of adsorbed water molecules observed in $3418.46\,cm^{-1}$ and $1629.47\,cm^{-1}$, respectively. The sharp peak in $1097.73\,cm^{-1}$ is owing to Si-O-Si stretching vibrations. The peak in $1460.85\,cm^{-1}$ is attribute to nitrogen embedded in TiO_2 lattice [30]. The peaks below $1000\,cm^{-1}$ is also corresponding to the Ti-O flexion vibrations [31].

3.3 UV-Vis DRS analysis

As shown in the DRS spectra of the prepared samples in Fig. 4, doping N and F in the TiO_2/SiO_2 lattice have resulted to a red shift in the absorption edges of undoped TiO_2/SiO_2. This fact indicates better photocatalytic activity of NFTS than undoped TiO_2/SiO_2, owing to the higher photo-generated electrons under visible light irradiation. The band gap of the prepared catalyst determined by the following equation: [32]
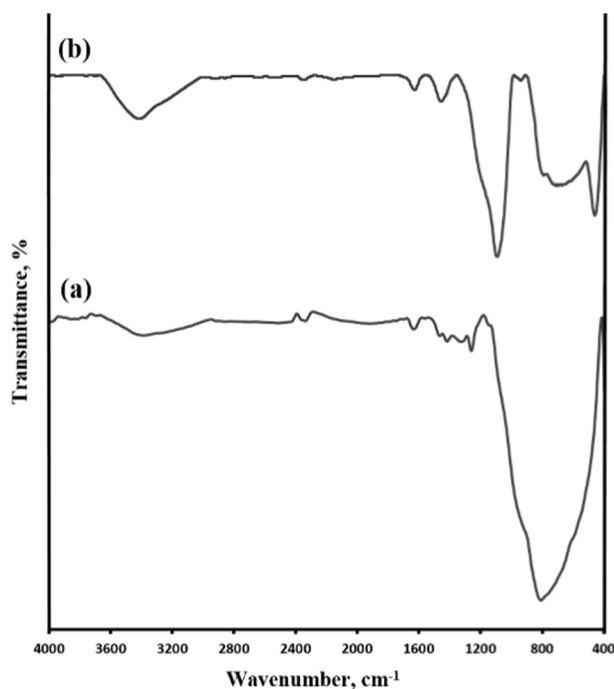
$$E_g = \frac{hC}{\lambda} \tag{3}$$

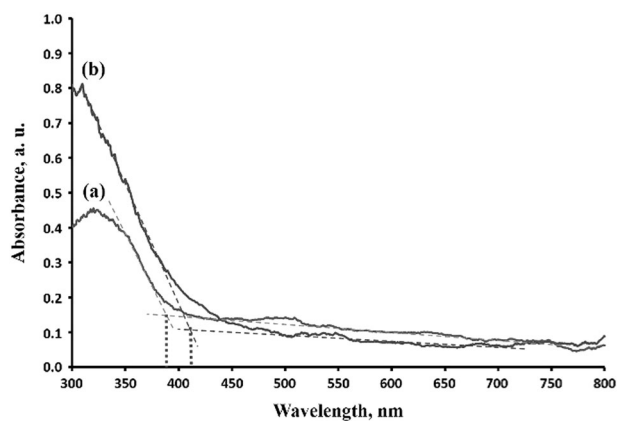**Fig. 3** FT-IR spectra of undoped TiO_2 **a** and NFTS **b**

Fig. 4 DRS spectra of undoped TiO_2/SiO_2 **a** and NFTS **b**

where E_g is the band gap, h is Planck's constant, C is light speed in vacuum and λ is the wavelength of the absorption edge in the related spectrum. The narrow band gap of the NFTS nanoparticles (2.99 eV) compare with the 3.17 eV of undoped TiO_2/SiO_2, has shown the advantage of doping these non-metals on the photocatalytic activity.

3.4 PL analysis

Photoluminescence is the process of light emission, originated from the recombination of electron-hole pairs [33]. There are two major pathways of electron/hole recombination, which result in the photoluminescence occurrence. Band-band PL process that attributed to the PL in shorter

wavelengths and excitonic PL process, which attributed to the PL in longer wavelengths. Generally, by investigating band-band PL, low PL intensity suggests less amount of recombination centers and consequently long lifetime of excited electrons. The photoluminescence behavior of the prepared nanocomposites was investigated with the excitation wavelength of 300 nm, in order to investigate the band-band PL process. As shown in Fig. 5, PL intensity of prepared NFTS nanoparticles is lower than undoped TiO_2/SiO_2 that suggest longer lifetime of photogenerated electrons.

3.5 FESEM and EDX analysis

Figure 6a, b shows the FESEM images of prepared photocatalysts calcinated at 500˚C. The particles shown to be globular and uniform with less agglomeration. As it is obvious, with the least particle size, the most photocatalytic activity is attainable. As it was shown in Fig. 6b doping N and F into TiO_2 lattice surpass crystalline growth and agglomeration of nanoparticles in contrast with undoped
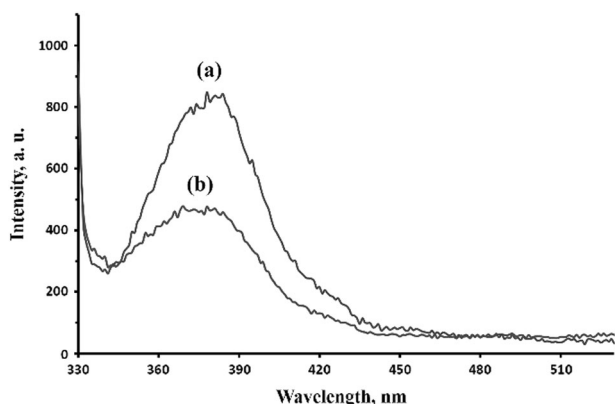
TiO_2, which revealed slight agglomeration and crystalline growth (Fig. 6a). EDX analysis was also shown in Fig. 5c, which indicates the successful doping of N, F, and Si into TiO_2 lattice.

3.6 TEM analysis

The TEM images of undoped TiO_2 and NFTS nanocomposites was shown in Fig. 7. The results shown the globular structure of the as-synthesized nanoparticles and were in good agreement with the FESEM results.

3.7 Nitrogen adsorption/desorption analysis

Figure 8 shows the nitrogen adsorption/desorption isotherm and the BJH pore size distribution curve of NFTS calculated from the adsorption branch (inset). The results shown a typical type IV-like with a type H2 hysteretic loop, corresponding to the presence of mesoporous materials owing to the IUPAC classification [34]. The effect of SiO_2 addition into the crystalline lattice of TiO_2 was also tabulated by BET method (Table 1). The results showed the significant effect of SiO_2 on increasing the interaction between the prepared substrate and pollutants.

3.8 Photocatalytic activities

The photodegradation experiments were performed on a mixture of $30\,mg\,L^{-1}$ of basic red 29, basic blue 41, basic yellow 51, and $5\,mg\,L^{-1}$ of hexavalent chromium. All experiments were performed under visible and solar irradiation. To attain the best degradation efficiencies, the effective parameters of pH, flow rate and photoreactor tubes angle against solar light were completely optimized. To confirm the performance of the prepared substrate, comparative experiments in the presence of undoped TiO_2/SiO_2,

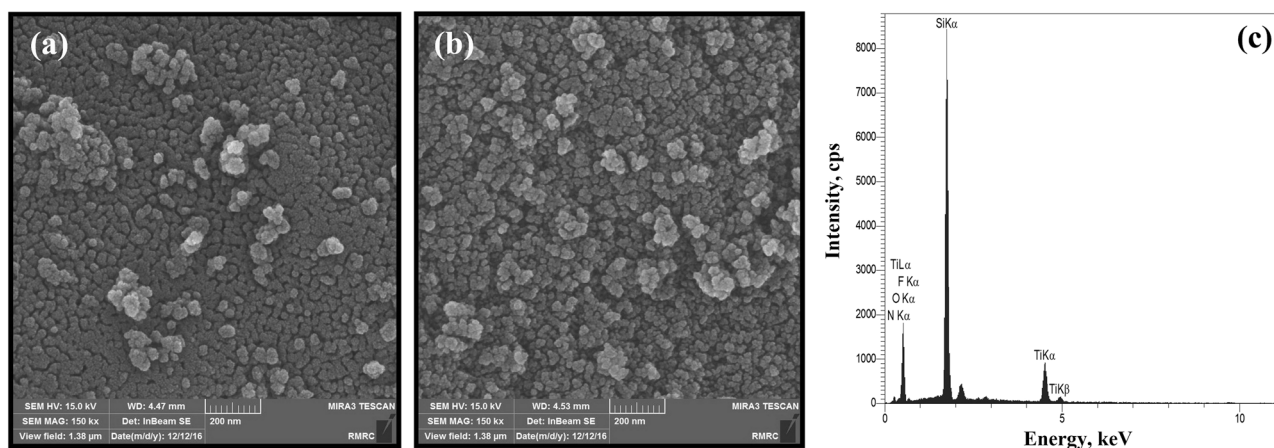**Fig. 5** PL spectra of undoped TiO_2/SiO_2 **a** and NFTS **b**

Fig. 6 FESEM images of undoped TiO_2 **a** NFTS **b** and EDX pattern of NFTS nanocomposites **c**
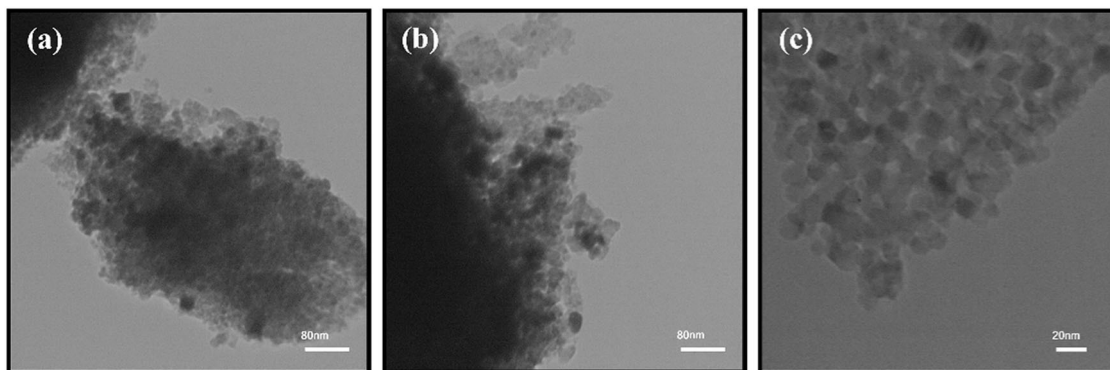
Fig. 7 TEM images of undoped TiO_2 **a** and NFTS nanocomposites **b** and **c**
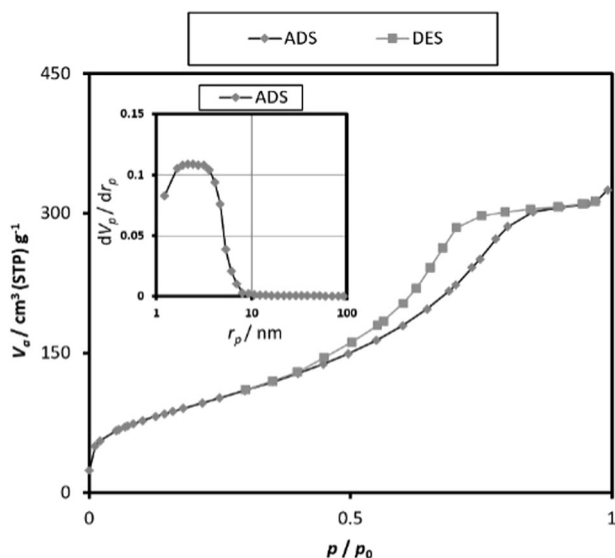

Fig. 8 N_2 adsorption/desorption isotherm of NFTS nanocomposites. Inset: BJH pore size distribution curve of NFTS

Table 1 Physical properties of prepared samples

Samples	BET surface area (S_{BET}), m^2 g^{-1}	Average pore diameter, nm
TiO_2	39.60	5.77
N-F-TiO_2	54.79	9.97
NFTS	344.77	5.81

in the absence of light source and in the absence of catalyst were accomplished.

3.9 Effect of pH

The effect of solution's pH was investigated at the pH of 3, 5, 7, and 9 (Fig. 9). Based on the results, it was concluded that the pH is one of the most important factors while working on a mixture of pollutants with complex matrices.
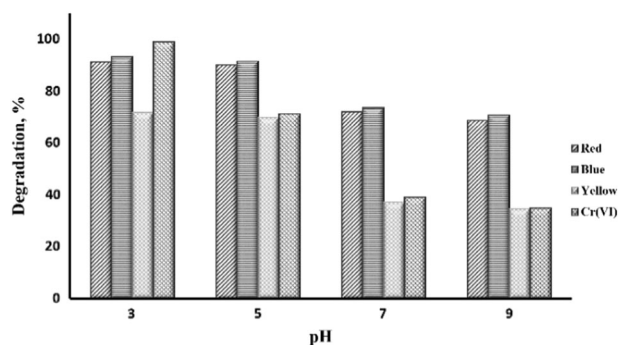

Fig. 9 Effect of pH on removal percentage of the pollutants upon NFTS

As it was observed, neutral and alkaline pH would decrease the removal efficiencies of both Cr (VI) and dyes. In other words, based on the following reaction, at acidic conditions the interaction between the Cr (VI) anions and the positive surface of TiO_2 surface, yields to increase the rate of Cr (VI) reduction:

$$Cr_2O_7^{2-} + 14H^+ + 6e_{cb}^- \rightarrow 2Cr^{3+} + 7H_2O \qquad (4)$$
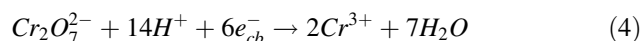
Although at the pH above 4–5, owing to the conversion of Cr (VI) to Cr (III), trivalent chromium tends to form a stable precipitate that would occupy the active sites of the prepared photocatalyst: [4, 27]

$$CrO_4^{2-} + 4H_2O + 3e_{cb}^- \rightarrow Cr(OH)_3 + 5OH^- \qquad (5)$$
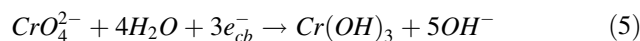
Consequently, owing to the highest photodegradation of dyes at acidic pH, the working pH for the further experiments was selected as 3 [35].

3.10 Effect of flow rate

Owing to the design of fabricated photoreactor, as a continuous-flow system, flow rate of the incoming pollutant
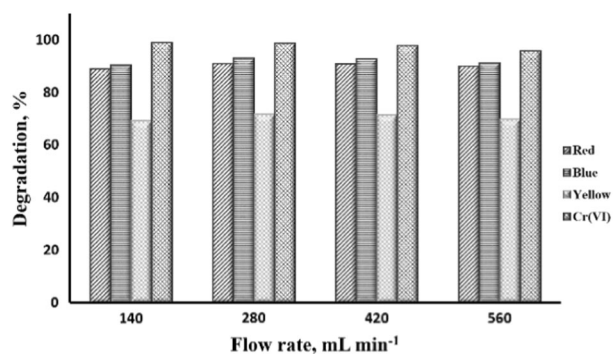
Fig. 10 Effect of flow rate on removal percentage of the pollutants upon NFTS

Fig. 11 Effect of photoreactor tubes' angle against sunlight on removal percentage of the pollutants upon NFTS

mixture current to the photoreactor was examined and optimized in four different rates of 140, 280, 420, and 560 mL min^{-1}. As shown in Fig. 10, there is not any significant difference between the results of each flow rate. However, it can suggest that at higher flow rates the interaction time between the pollutants and the surface of the catalyst is not enough to reach highest removal efficiencies. Alternatively, at lower flow rates, because of the presence of hexavalent chromium as a heavy metal, the chance of trapping it in the active sites of the catalyst would be increased and results to decrease of removal efficiencies of both organic and inorganic pollutants. Subsequently, 280 mL min^{-1} was selected as the optimum flow rate for the further experiments.

3.11 Effect of photoreactor tube's angle against solar irradiation

One of the most important factors influenced on the efficiencies of continuous-flow reactors under solar irradiation is the angle of the tubes containing wastewater against sun. To investigate the effect of this parameter in treatment process, the tubes' support was designed adjustable in three different angles of 30°, 45°, and 60° against sunlight. As it was shown in Fig. 11, at 30° because of the inadequate income solar irradiation, the degradation and reduction efficiencies was not so high. At the other hand, at 60° decrease in photodegradation of the dyes and increase in the rate of Cr (VI) reduction were occurred. To verify the fast chromium removal, total Cr amount was measured by flame atomic absorption spectroscopy (FAAS) method on the treated sample. The results in Table 2 indicated that decrease in the chromium amount was occurred because of trapping and occupying the active sites of the substrate that resulted to decrease in the removal efficiencies of the dyes. Consequently, to gain a balance between the photodegradation and reduction efficiencies, the 45° was chosen for the further experiments as optimum.

The photodegradation experiments were performed under visible and solar light on 1000 mL mixture of the
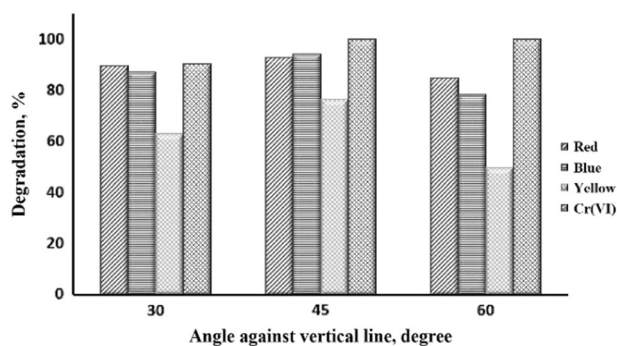
Table 2 Cr (VI) determination by FAAS method at different angles

Angle against solar irradiation	30°	45°	60°
Initial Cr (VI) concentration (mg L^{-1})	5.00	5.00	5.00
Cr (VI) concentration after the process (mg L^{-1})	0.49	0.00	0.00
Removal (%)	90.28	100.00	100.00

pollutants and sampling was accomplished every 2 hours to control the process. As shown in Fig. 12a codoping N, F, and Si into the TiO$_2$ lattice were meaningfully increased the photocatalytic activity of the prepared substrate under visible light. Figure 12b also shows the removal efficiencies of the pollutant mixture under solar irradiation. Parallel experiments were similarly accomplished in the absence of photocatalyst to realize the stability of the pollutants in front of light sources. As it is evident, the pollutants are extremely stable in the environment and it prove the beneficial point of using such systems to decontaminate wastewaters. To understand any adsorption of the pollutants on the prepared substrate while the photodegradation process, the experiment was accomplished in the dark conditions (Fig. 13). The results showed no significant adsorption on the surface and the occurred amount was assumed owing to the porosity of the glass beads.

One of the great concerns of using such systems under the green energy of sun is capability of employing under either clear sky or cloudy one. To scrutinize the potential performance of the fabricated photoreactor in different climate conditions, the photodegradation experiments were executed under semi-cloudy sky. The results, in Fig. 14, confirmed great promising activity of the designed system under solar irradiation even in cloudy sky conditions.

Total organic carbon (TOC) analysis was also accomplished on the samples, prior and subsequent the treatment process, to understand the amount of decreased organic carbon of the prepared standard wastewater solution. As it is clear, the reducing amount of the TOC percentage after the treatment process, declares good performance of the system
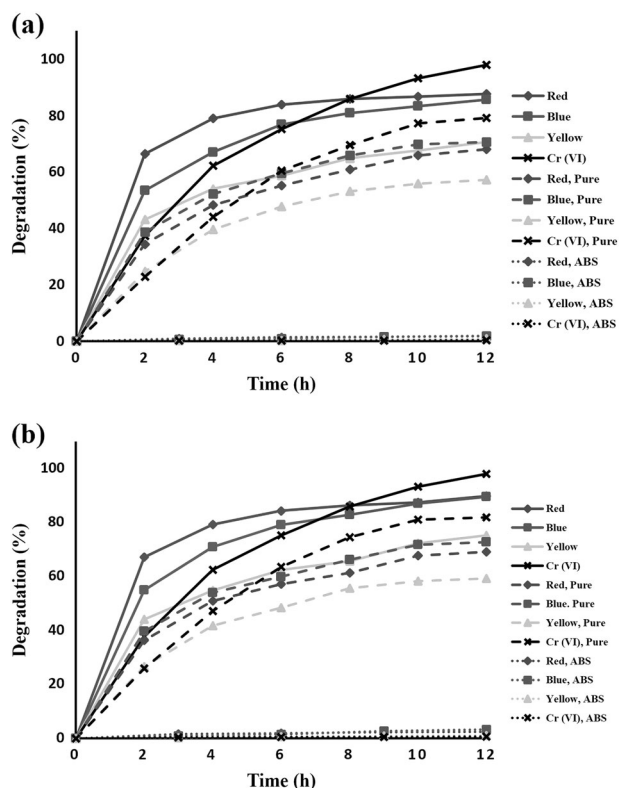
(a)

(b)

Fig. 12 Removal percentages under visible light irradiation **a** and solar irradiation **b** in the presence and absence of NFTS; Pure: TiO_2/SiO_2; ABS: absence of photocatalyst
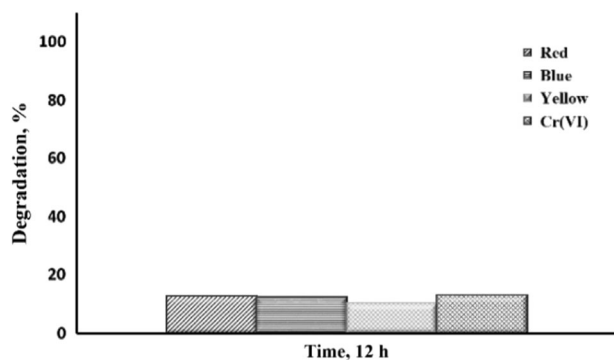

Fig. 13 Removal efficiencies of the pollutants in dark condition in the presence of NFTS

Fig. 14 Removal percentages under solar irradiation at semi-cloudy condition

4 Conclusion

A new TiO_2/SiO_2 nanocomposite doped with nitrogen and fluorine immobilized on a surface was used for synergistic removal of a mixture consist of Cr (VI) and three azo dyes in a fabricated photoreactor under visible and sunlight. The nanoparticles were synthetized using simple sol-gel method. In order to highly stabilize the nanoparticles on the glass beads' surface and prevent the mixing between the nanoparticles and treated wastewater, dip coating, and heat attachments methods were applied subsequent the etching process. The optimum angle of the photoreactor's tubes against solar irradiation was also one of the most important factors that was investigated. The outdoor performance of the designed system was also evaluated under semi-cloudy sky. The results showed the significant efficiency of the system in simultaneous removal of hexavalent chromium and azo dyes and confirmed the auspicious activity of the fabricated system under visible and solar irradiations at different outdoor climate conditions.

Compliance with ethical standards

Conflict of interest The authors declare that they have no conflict of interest.

References

1. Anpo M, Dohshi S, Kitano M et al. (2005) The preparation and characterization of highly efficient titanium oxide–based photofunctional materials Annu Rev Mater Res 35:1–27
2. Wu Y, Xing M, Tian B et al. (2010) Preparation of nitrogen and fluorine co-doped mesoporous TiO_2 microsphere and photodegradation of acid orange 7 under visible light. Chem Eng J 162:710–717

in removal of the organic wastewater pollutants. The results showed 54.87% and 58.53% decrease in the TOC amount of the samples under visible and solar irradiation, respectively. To verify the reduction of hexavalent chromium, total chromium amount of the treated sample was measured by FAAS analysis. Because of the porosity of the glass beads, it was expected to be an insignificant adsorption of this heavy metal on the surface and it was determined to be $1.01\ mg\ L^{-1}$.
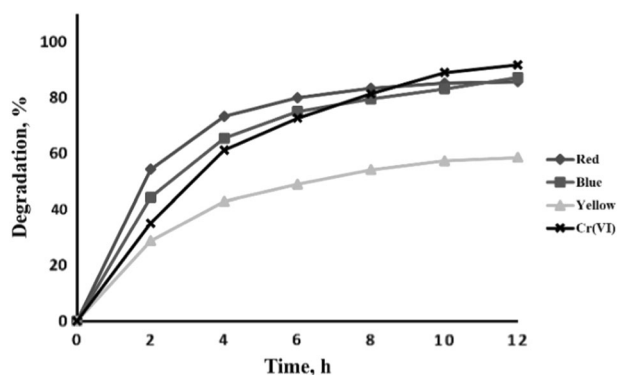
3. Wang Q, Chen X, Yu K et al. (2013) Synergistic photosensitized removal of Cr(VI) and Rhodamine B dye on amorphous TiO$_2$ under visible light irradiation. J Hazard Mater 246–247:135–144

4. Papadam T, Xekoukoulotakis NP, Poulios I, Mantzavinos D (2007) Photocatalytic transformation of acid orange 20 and Cr(VI) in aqueous TiO$_2$ suspensions. J Photochem Photobiol A Chem 186:308–315

5. Ni M, Leung MKHH, Leung DYCC, Sumathy K (2007) A review and recent developments in photocatalytic water-splitting using TiO$_2$ for hydrogen production Renew Sustain Energy Rev 11:401–425

6. Zhang J, Zhou P, Liu J, Yu J (2014) New understanding of the difference of photocatalytic activity among anatase, rutile and brookite TiO$_2$. Phys Chem Chem Phys 16:20382–20386

7. Pelaez M, Nolan NT, Pillai SC et al. (2012) A review on the visible light active titanium dioxide photocatalysts for environmental applications. Appl Catal B Environ 125:331–349

8. Dette C, Pérez-Osorio MA, Kley CS et al. (2014) TiO$_2$ anatase with a bandgap in the visible region. Nano Lett 14:6533–6538

9. Bangkedphol S, Keenan HE, Davidson CM et al. (2010) Enhancement of tributyltin degradation under natural light by N-doped TiO$_2$ photocatalyst. J Hazard Mater 184:533–537

10. Zhang G, Zhang YC, Nadagouda M et al. (2014) Visible light-sensitized S, N and C co-doped polymorphic TiO$_2$ for photocatalytic destruction of microcystin-LR. Appl Catal B Environ 144:614–621

11. Asahi R, Morikawa T, Ohwaki T, Taga Y. (2001) Visible-light photocatalysis in nitrogen-doped titanium oxides. Science 293:269–271

12. Dozzi MV, Selli E (2013) Doping TiO$_2$ with p-block elements: effects on photocatalytic activity. J Photochem Photobiol C Photochem Rev 14:13–28

13. Gombac V, De Rogatis L, Gasparotto A et al. (2007) TiO$_2$ nanopowders doped with boron and nitrogen for photocatalytic applications. Chem Phys 339:111–123

14. Ding X, Song X, Li P et al. (2011) Efficient visible light driven photocatalytic removal of NO with aerosol flow synthesized B, N-codoped TiO$_2$ hollow spheres. J Hazard Mater 190:604–612

15. Pol R, Guerrero M, Garcia-Lecina E et al. (2016) Ni-, Pt- and (Ni/Pt)-doped TiO$_2$ nanophotocatalysts: a smart approach for sustainable degradation of Rhodamine B dye. Appl Catal B Environ 181:270–278

16. Sun H, Zhou G, Liu S et al. (2013) Visible light responsive titania photocatalysts codoped by nitrogen and metal (Fe, Ni, Ag, or Pt) for remediation of aqueous pollutants. Chem Eng J 231:18–25

17. Khalilian H, Behpour M, Atouf V, Hosseini SN (2015) Immobilization of S, N-codoped TiO$_2$ nanoparticles on glass beads for photocatalytic degradation of methyl orange by fixed bed photoreactor under visible and sunlight irradiation. Sol Energy 112:239–245

18. Yao N, Wu C, Jia L et al. (2012) Simple synthesis and characterization of mesoporous (N, S)-codoped TiO$_2$ with enhanced visible-light photocatalytic activity. Ceram Int 38:1671–1675

19. Yu J, Zhou M, Cheng B, Zhao X (2006) Preparation, characterization and photocatalytic activity of in situ N,S-codoped TiO$_2$ powders. J Mol Catal A Chem 246:176–184

20. Xie Y, Li Y, Zhao X (2007) Low-temperature preparation and visible-light-induced catalytic activity of anatase F-N-codoped TiO$_2$. J Mol Catal A Chem 277:119–126

21. Pang D, Qiu L, Wang Y et al. (2015) Photocatalytic decomposition of acrylonitrile with N–F codoped TiO$_2$/SiO$_2$ under simulant solar light irradiation. J Environ Sci 33:169–178

22. Anderson C, Bard AJ (1995) An improved photocatalyst of TiO$_2$/SiO$_2$ prepared by a Sol-Gel synthesis. J Phys Chem 99:9882–9885

23. Mahesh KPO, Kuo DH, Huang BR et al (2014) Chemically modified polyurethane-SiO$_2$/TiO$_2$ hybrid composite film and its reusability for photocatalytic degradation of Acid Black 1 (AB 1) under UV light Appl Catal A Gen 475:235–241

24. Islam S, Rahman RA, Othaman Z et al. (2013) Preparation and characterization of crack-free sol-gel based SiO$_2$-TiO$_2$ hybrid nanoparticle film. J Sol-Gel Sci Technol 68:162–168

25. Yu JC, Yu J, Ho W et al. (2002) Effects of F- doping on the photocatalytic activity and microstructures of nanocrystalline TiO$_2$ powders. Chem Mater 14:3808–3816

26. Schrank SG, Jose HJ, Moreira RFPM (2002) Simultaneous photocatalytic Cr(VI) reduction and dye oxidation in a TiO$_2$ slurry reactor. J Photochem Photobiol A Chem 147:71–76

27. Yang Y, Wang G, Deng Q et al. (2014) Microwave-assisted fabrication of nanoparticulate TiO$_2$ microspheres for synergistic photocatalytic removal of Cr(VI) and methyl orange. ACS Appl Mater Interfaces 6:3008–3015

28. Xie M, Jing L, Zhou J et al. (2010) Synthesis of nanocrystalline anatase TiO$_2$ by one-pot two-phase separated hydrolysis-solvothermal processes and its high activity for photocatalytic degradation of rhodamine B. J Hazard Mater 176:139–145

29. File PD (1997) Card No. 21−1272. JCPDS-International Cent Diffr Data, Swart

30. Kaur N, Kaur S, Singh V (2016) Preparation, characterization and photocatalytic degradation kinetics of Reactive Red dye 198 using N, Fe codoped TiO$_2$ nanoparticles under visible light. Desalin Water Treat 57:9237–9246

31. Hamadanian M, Reisi-Vanani A, Behpour M, Esmaeily AS (2011) Synthesis and characterization of Fe,S-codoped TiO$_2$ nanoparticles: application in degradation of organic water pollutants. Desalination 281:319–324

32. O'Regan B, Grätzel M (1991) A low-cost, high-efficiency solar cell based on dye-sensitized colloidal TiO$_2$ films. Nature 353:737–740

33. Luo S, Xiao Y, Yang L et al. (2011) Simultaneous detoxification of hexavalent chromium and acid orange 7 by a novel Au/TiO$_2$ heterojunction composite nanotube arrays. Sep Purif Technol 79:85–91

34. Alothman ZA (2012) A review: fundamental aspects of silicate mesoporous materials. Mater (Basel) 5:2874–2902

35. Konstantinou IK, Albanis TA (2004) TiO$_2$-assisted photocatalytic degradation of azo dyes in aqueous solution: Kinetic and mechanistic investigations: a review. Appl Catal B Environ 49:1–14